Electrodynamic Force, Casimir Effect, and Stiction Mitigation in Silicon Carbide Nanoelectromechanical Switches

Rui Yang,* Jiang Qian,* and Philip X.-L. Feng*

Logic switches enabled by nanoelectromechanical systems (NEMS) offer abrupt on/off-state transition with zero off-state leakage and minimal subthreshold swing, making them uniquely suited for enhancing mainstream electronics in a range of applications, such as power gating, high-temperature and high-voltage logic, and ultralow-power circuits requiring zero standby leakage. As NEMS switches are scaled with genuinely nanoscale gaps and contacts, quantum mechanical electrodynamic force (EDF) takes an important role and may be the ultimate cause of the plaguing problem of stiction. Here, combined with experiments on three-terminal silicon carbide (SiC) NEMS switches, a theoretical investigation is performed to elucidate the origin of EDF and Casimir effect leading to stiction, and to develop a stiction-mitigation design. The EDF calculation with full Lifshitz formula using the actual material and device parameters is provided. Finite element modeling and analytical calculations demonstrate that EDF becomes dominant over elastic restoring force in such SiC NEMS when the switching gap shrinks to a few nanometers, leading to irreversible stiction at contact. Artificially corrugated contact surfaces are designed to reduce the contact area and the EDF, thus evading stiction. This rational *surface engineering* reduces the EDF down to 4% compared with the case of unengineered, flat contact surfaces.

1. Introduction

Contact-mode logic switches (relays) enabled by micro/nanoelectromechanical systems (M/NEMS) have been under considerable exploration for high-temperature logic and ultralow-power circuits to supplement silicon electronics, owing to the fundamental merits of the ideally abrupt switching characteristics

Prof. R. Yang, Dr. J. Qian, Prof. P. X.-L. Feng
Department of Electrical Engineering and Computer Science
Case School of Engineering
Case Western Reserve University
Cleveland, OH 44106, USA
E-mail: rui.yang@sjtu.edu.cn; jiang.qian@post.harvard.edu;
philip.feng@ufl.edu
Prof. R. Yang
University of Michigan–Shanghai Jiao Tong University Joint Institute
Shanghai Jiao Tong University
Shanghai 200240, China
Prof. P. X.-L. Feng
Department of Electrical and Computer Engineering
Herbert Wertheim College of Engineering
University of Florida
Gainesville, FL 32611, USA

with zero subthreshold swing, zero off-state leakage, as well as harsh-environment compatibility.[1–6] In particular, endowed with outstanding mechanical properties and chemical inertness, silicon carbide (SiC) NEMS switches have exhibited great promises for logic functions and circuit building blocks, with experimental demonstrations of high-temperature NEMS switching up to 500 °C, low-voltage operation, and over 10^7 cycles of hot switching, suggesting that SiC is resistant to wearing out.[6–9] As the device size and switching gap are scaled down, new physical phenomena in the quantum regime, including new interactions and forces, emerge and play more important roles to complicate the design and performance of M/NEMS devices. For switches where genuinely nanoscale contacts are crucial determinants of the performance, stiction between interfaces due to quantum mechanical electrodynamic force (EDF) or Casimir effect has become an ultimate factor compromising the device.[10,11]

EDF, usually known as van der Waals force (at shorter range) or Casimir force (at longer range), originates from the modification of quantum and thermal fluctuations of the electromagnetic (EM) field due to dielectric material boundaries.[12–14] Quantum fluctuations of EM field are highly intriguing quantum effects with a number of observable consequences at mesoscopic scale, in micro/nanofabricated devices. Recently, heat transfer through phonon coupling across vacuum due to quantum fluctuations has been reported, which brings new discussions in thermodynamics.[15] In nanomechanics, quantum fluctuations of EM field can lead to a force between two neutral objects separated by vacuum, also called Casimir effect.[16] The uncertainty principle requires zero-point energy in vacuum and gives rise to virtual photons, which results in attractive EDF because of higher EM mode density in free space than that between the two parallel plates.[17–19] The force is often negligible at the scale of microns and above; however, it grows into a significant force as the distance becomes smaller than 10 nm. Since fields undergo quantum fluctuations, EDF is unavoidable in MEMS and NEMS switches; especially, when two smooth surfaces are in good contact, the distance between them is typically extremely small (close to the lattice constant), leading to a quite large EDF. When the EDF is larger than the elastic restoring force, stiction will occur and the device cannot switch again. NEMS switches can often have relatively small rigidity

and restoring force, therefore, it is essential to reduce the EDF to ensure the device functionality. A lot of theoretical and experimental research progress in EDF has been reported, including computational methods, experiments to precisely measure the EDF, and inducing repulsive forces by immersing the two plates in adequate fluid.[20–34] Furthermore, recent progress in on-chip actuation and sensing for Casimir force measurement, as well as the demonstration of non-monotonic Casimir force using complex shapes, provides important guidelines and new possibilities for reducing the EDF using shape or geometry engineering.[35,36] In contact-mode M/NEMS switches, more extensive investigations, including complete analysis of the origin of the EDF using experimentally relevant device dimensions, and methods for systematically reducing the chance of stiction using surface engineering, are necessary and imperative, to avoid stiction-induced failure and to extend the lifetime of M/NEMS switches.

In this work, we systematically examine the nature of EDF and the procedure of calculating EDF in realistic geometries of three-terminal SiC NEMS switches, and propose the engineering of surface grooves to dramatically reduce the EDF. We first experimentally demonstrate 3C-SiC NEMS switches and the stiction problem during device measurements. Working in the framework of Lifshitz theory of electrodynamic interaction, we then employ the material-specific, frequency-dependent dielectric functions, obtained from experimental data (for gold) and ab initio calculations (for SiC), to compute the EDF.[37–41] We show that given the same device geometry, the EDF between gold surfaces is larger than that between SiC surfaces, suggesting a higher chance of stiction for gold devices. We then demonstrate that, when two atomically smooth flat surfaces are put into contact, the EDF will cause so large a surface attraction that the EDF will dominate over the elastic restoring force and stiction will occur within a large range of device parameters. We then discuss about the possibility of engineering the surface roughness to reduce the EDF when two surfaces are in contact. We show that by producing a corrugated surface with sinusoidal modulation, we can reduce the EDF between a corrugated surface and a smooth surface to only

4% compared to the EDF between two smooth surfaces, due to the much reduced contact area. We also use finite element method (FEM) simulation to demonstrate the EDF reduction using surface grooves for devices with experimentally relevant geometries and surface roughness, which suggests that such surface engineering provides an important method toward the goal of realizing stiction-free NEMS switches. Furthermore, such surface engineering technique has very high potential to extend toward reducing stiction forces in other types of contact-mode M/NEMS switches.

2. Results and Discussions

As shown in **Figure 1**a, for two neutral plates placed parallel to each other, quantum fluctuations of the EM field can be described by virtual photons, and for two identical materials with vacuum in between, the EM mode density outside the cavity is higher than that inside the cavity, leading to an attractive force between the two plates. For a three-terminal SiC NEMS switch, when the cantilever beam (source terminal, S) is freely suspended, the switch is in the Off state (Figure 1b,c), and when the cantilever is in contact with the local drain (D) electrode, the switch is in the On state (Figure 1d,e). At contact, if the EDF between the cantilever and the local drain (D) is higher than the elastic restoring force of the cantilever, then the cantilever is permanently stuck to the local drain, leading to device failure (Figure 1e). This could severely limit the lifetime of these NEMS switches.

To experimentally observe the stiction effect, we fabricate SiC NEMS switches and perform electrical measurements. We use 3C-SiC film with thickness of 500 nm grown on oxidized silicon (Si) substrates using low-pressure chemical vapor deposition (LPCVD) and heavily doped with NH_3 gas.[42] The switches are patterned using electron beam lithography (EBL) followed by dry etching of SiC, resulting in switches with cantilever beam width down to 200 nm. Finally, the SiC cantilevers are released in vapor hydrofluoric acid (HF). Then we perform electrical characterization on these SiC NEMS switches at room
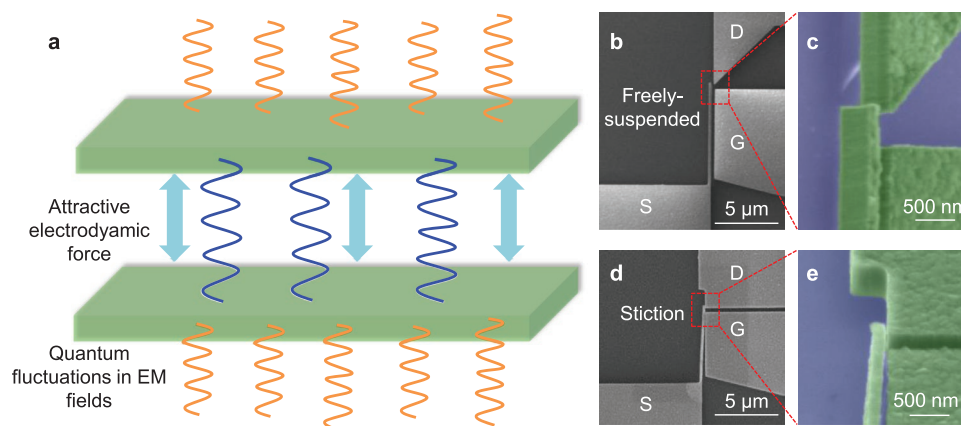

Figure 1. Illustration of electrodynamic force (EDF) and stiction in SiC NEMS switches. a) A 3D schematic of the formation of the attractive EDF. b–e) Scanning electron microscopy (SEM) images of the SiC NEMS switches, showing b) a freely suspended SiC nanocantilever (top view), and c) color-enhanced SEM image depicting the zoom-in view of (b); d) a SiC nanocantilever in stiction (top view), and e) colored SEM image depicting the zoom-in view of (d).
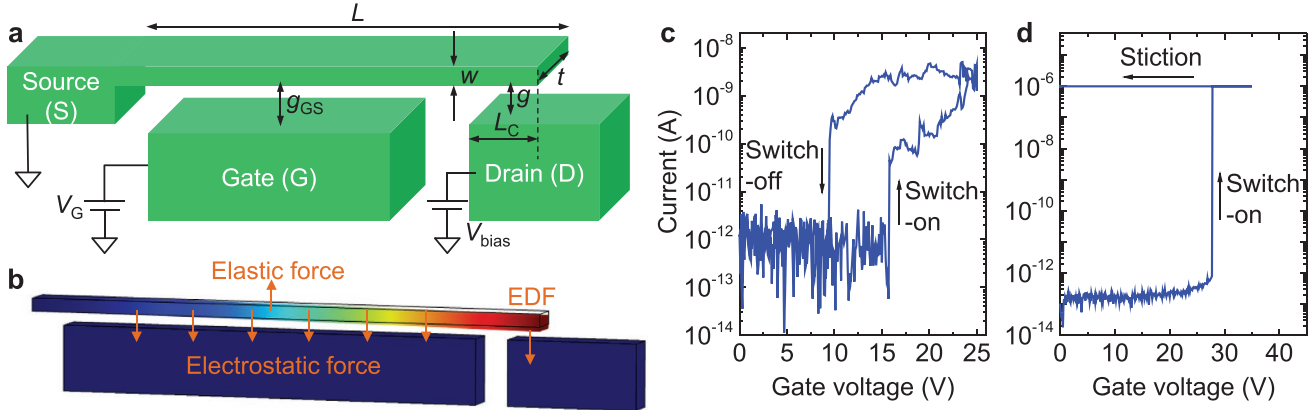
ADVANCED
SCIENCE NEWS
www.advancedsciencenews.com

NANO · MICRO
small
www.small-journal.com

Figure 2. Effects of EDF in SiC NEMS switches. a) A 3D schematic of a three-terminal SiC NEMS switch, showing the voltage biasing scheme and the definition of geometry, where L is the length, w is the width, and t is the thickness of the cantilever (set by the SiC film thickness), g_{GS} is the gap between the cantilever (S) and the gate (G), g is the gap between the cantilever (S) and the local drain (D), and L_C is the overlapping length defining the contact length between the cantilever and the drain. b) FEM simulation showing the cantilever deflection, with illustrations of all the forces on the cantilever beam. c,d) Electrical measurement results for two typical SiC NEMS switches, showing c) normal operation with switch-on and switch-off, for a switch with $L = 10$ μm, $w = 250$ nm, and $t = 500$ nm, and d) stiction for another device with $L = 8$ μm, $w = 200$ nm, and $t = 500$ nm, with drain voltage V_{bias} of 0.1 V.

temperature (300 K). During the switching of a three-terminal NEMS switch, the voltage is applied to the gate (G) electrode, with the source (S) electrode grounded (connected to the movable cantilever beam), and a small bias voltage at the local drain (D) electrode (**Figure 2**a). FEM simulation of the switching process is performed to capture the deflection profile of the beam due to the electrostatic force (Figure 2b). After mechanical switch-on, during normal switching cycles, the beam switches off at a lower gate voltage due to the EDF (Figure 2c). The elastic restoring force of the cantilever is larger than the EDF, so the cantilever can pull away from the contact. For another switch after contact, the EDF is larger than the elastic restoring force, so the cantilever is permanently stuck to the drain, and the current does not drop as the gate voltage sweeps back, indicating device failure (Figure 2d). While intuitively it is possible to engineer the rigidity of the beam to obtain a larger restoring force and reduce the chance of stiction, this will inevitably result in a large switch-on voltage, which is not desirable. As we will show later, the EDF easily dominates over the restoring force after contact, so surface engineering is more promising for reducing stiction.

In the limit where the radius of curvature of every boundary involved is much larger than the distance between surfaces, the Lifshitz formula for dielectric materials in parallel plate geometry can be applied. The electrodynamic interaction energy per unit area between two semi-infinite plates (labeled as "A" and "B") separated by medium "m" of thickness g at temperature T is:

$$G_{AmB}(g,T) = -(k_B T)/(8\pi g^2)$$
$$\sideset{}{'}\sum_{n=0}^{\infty} \int_{r_n}^{\infty} x \ln\left[\left(1 - \Delta_{Am}^{\mu}\Delta_{Bm}^{\mu}e^{-x}\right)\left(1 - \Delta_{Am}^{\varepsilon}\Delta_{Bm}^{\varepsilon}e^{-x}\right)\right]dx \quad (1)$$

where $\Delta_{jm}^{\varepsilon} = \dfrac{x_j \varepsilon_m(i\xi_n) - x_m \varepsilon_j(i\xi_n)}{x_j \varepsilon_m(i\xi_n) + x_m \varepsilon_j(i\xi_n)}$, $\Delta_{jm}^{\mu} = \dfrac{x_j \mu_m(i\xi_n) - x_m \mu_j(i\xi_n)}{x_j \mu_m(i\xi_n) + x_m \mu_j(i\xi_n)}$,

j = A or B, $\hbar\xi_n = 2\pi k_B T$, ξ_n is the imaginary frequency,

$x_j = \sqrt{x^2 + r_n^2\left[\dfrac{\varepsilon_j(i\xi_n)\mu_j(i\xi_n)}{\varepsilon_m(i\xi_n)\mu_m(i\xi_n)} - 1\right]}$, $r_n = \dfrac{2g\xi_n}{c}\sqrt{\varepsilon_m(i\xi_n)\mu_m(i\xi_n)}$, $x_m = x$.

Here $\sideset{}{'}\sum$ means that the $n = 0$ term of the sum is multiplied by 1/2. We study the EDF between two semi-infinite planes with the same nonmagnetic material, separated by vacuum or air. Thus $\mu_m = \mu_A = \mu_B = 1$, and $\varepsilon_m = 1$, $\varepsilon_A = \varepsilon_B = \varepsilon$. Once we have the interaction energy $G_{AmB}(g,T)$, the EDF can be obtained straightforwardly by:

$$F_{AmB}(g,T) = -\partial G_{AmB}(g,T)/\partial g \quad (2)$$

The EDF between two objects of the same kind of material separated by vacuum can be proved to be always attractive.

Crucial to this calculation is the dielectric function at temperature-determined imaginary frequencies ξ_n, which can be calculated from the Kramers–Kronig formula that relates the real and imaginary frequency response functions:

$$\varepsilon(i\xi_n) = 1 + \frac{2}{\pi}\int_0^{\infty} d\omega_R \frac{\omega_R \varepsilon_2(\omega_R)}{\omega_R^2 + \xi_n^2} \quad (3)$$

We compare the dielectric functions of both SiC and gold. In Equation (3), we use as input $\varepsilon_2(\omega_R)$, the imaginary part of the dielectric response function at real frequencies ω_R, which determines the absorption of light at this frequency. We use the $\varepsilon_2(\omega_R)$ data obtained from experiments for gold[37] and ab initio calculations for SiC,[37,39–41] as shown in **Figure 3**. Other measurement data of $\varepsilon_2(\omega_R)$ for gold and SiC also show similar values.[43–45] The large $1/\omega_R$ singularity near the origin for gold is consistent with the Drude model for electron transport below the plasma frequency for metal. Compared with the semiconductor material SiC, this divergence of metallic gold means the low-frequency EM field must vanish at the boundary of the plate, thus enabling gold devices to modify EM fluctuations more strongly than SiC, leading to a larger EDF.

With the dielectric functions, we further calculate the EDF in gold and SiC structures. In **Figure 4**a,b, we show the EDF per unit area between two parallel plates separated by distance g, for gold and SiC, respectively. The plate surfaces are assumed to be atomically smooth in this calculation. The other
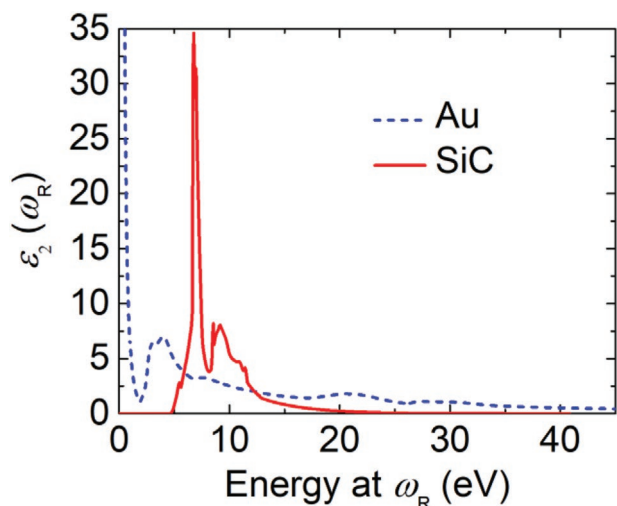
Figure 3. The imaginary part of the frequency-dependent dielectric functions at real frequencies, for gold (blue dashed line, from experimental data), and SiC (red solid line, obtained from ab initio calculations).

dimensions of the two surfaces are assumed to be much larger than g, thus they can be treated as semi-infinite surfaces. This condition can often be satisfied in NEMS and MEMS switches where the gap between the surfaces is much smaller than the dimension of the devices involved. In such case the EDF per unit area manifests itself as an attractive pressure P. At short distance or small separation ($g \leq 10$ nm for gold and $g \leq 30$ nm for SiC), the EDF in both gold and SiC exhibit EDF $\propto g^{-3}$, whereas at long distance ($g \geq 200$ nm for gold, and $g \geq 70$ nm for SiC), the EDF shows EDF $\propto g^{-4}$. In many NEMS and MEMS applications, much of the interesting physics happens precisely at the intermediate distance where EDF cannot be simply approximated by either g^{-3} or g^{-4} power law dependence.[46,47] The error from either g^{-3} or g^{-4} approximation can be as large as a factor of two, which does not show clearly in the log–log

plot in Figure 4. A full Lifshitz treatment of this force is important in such a situation, using Equations (1) and (2).

For SiC plates, the EDF per unit area is also compared with the electrostatic force per unit area in SiC NEMS switches. The electrostatic force per unit area for parallel plate capacitors is simply obtained using $F_{elec}/A = \frac{\varepsilon_0}{2g^2}V_G^2$, where A is the overlapping area between the gate and the beam, ε_0 is the vacuum permittivity, and V_G is the gate voltage. We show that the EDF per unit area is larger than the electrostatic force per unit area at 1 V for distances below 1.5 nm, and becomes smaller than F_{elec}/A for distances above 1.5 nm. The EDF per unit area is also compared with the atmosphere pressure, showing that it can easily be stronger than atmosphere pressure for distances below 4 nm.

To gain a better understanding of the typical magnitude of the total EDF in NEMS switches close to contact, we further compare the EDF in gold and SiC at small surface distances. In **Figure 5**, we present the EDF calculation between the nanobeams and their local drain electrodes, using experimentally relevant device dimensions of $L = 8$ μm, $w = 200$ nm. The contact area, or the overlapping area between the cantilever and the local drain is 500 nm × 500 nm = 0.25 μm², which is used to calculate the EDF, still for the atomically smooth surfaces. As discussed above, the divergence of $\varepsilon_2(\omega_R)$ in gold at low frequency means that a gold device boundary modifies the EM fluctuations more strongly than SiC. As seen in Figure 5, this gives rise to a stronger electrodynamic attraction force between two gold surfaces than that between two SiC ones. Here the calculation assumes atomically smooth and flat surfaces, so the overlapping area of 0.25 μm² is assumed to be the contact area. Further, the Young's modulus of gold (79 GPa) is smaller than SiC (401 GPa), leading to a smaller restoring force for the gold cantilever compared with the SiC cantilever. Therefore, it will be advantageous to use SiC cantilevers instead of gold cantilevers, for reducing the chance of stiction failure in NEMS switches.
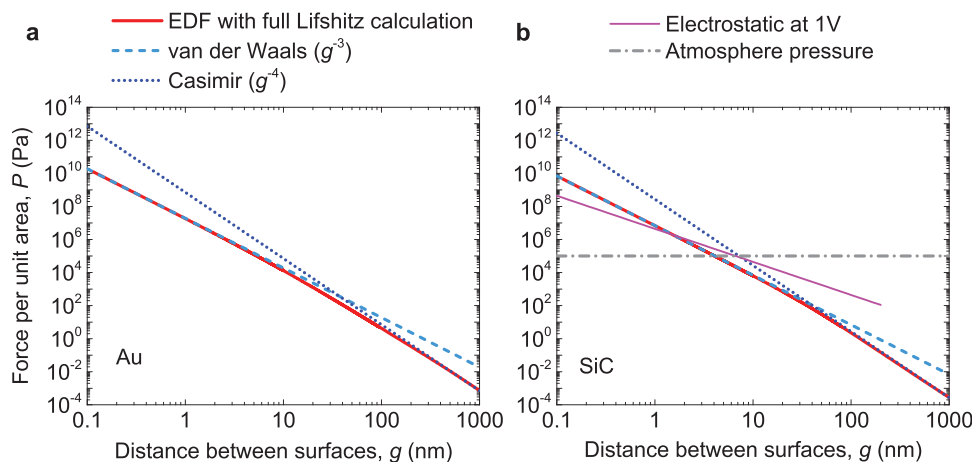

Figure 4. Calculated full EDF per unit area between two semi-infinite gold and SiC plates. a) EDF per unit area for gold, calculated from Lifshitz formula (red line), with fitting to the non-retarded EDF $\propto g^{-3}$ at short range (light blue dashed line), and the retarded EDF $\propto g^{-4}$ at long range (blue dotted line). b) Calculation of EDF per unit area for SiC with the same color coding as in (a), and is also compared with the electrostatic force per unit area at 1 V actuation (magenta line), and the atmosphere pressure (gray dash dot line).
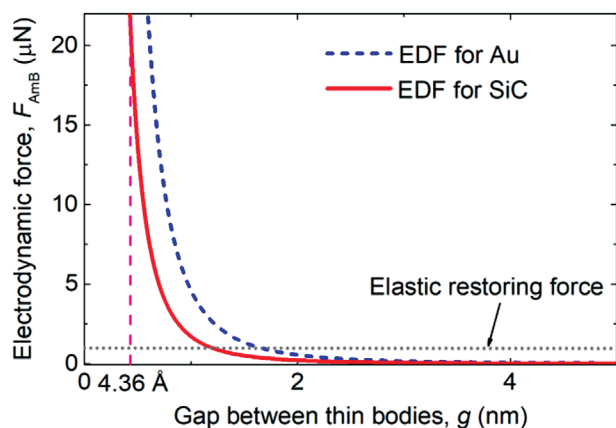
**ADVANCED
SCIENCE NEWS**

www.advancedsciencenews.com

NANO · MICRO

small

www.small-journal.com

Figure 5. Comparison of EDF as a function of gap, between two identical cantilevers and the local drains, with the cantilever made of gold (blue dashed line) and SiC (red solid line), and realistic dimension of $L = 8$ μm, $w = 200$ nm, and $t = 500$ nm, assuming contact area of 500 nm × 500 nm = 0.25 μm². The elastic restoring force of SiC cantilever is shown as a reference (grey dotted line). The SiC lattice constant (4.36 Å) is shown by the magenta dashed vertical line.

Using the better material (such as SiC) alone is not enough to avoid stiction. The EDF here is very strong, especially when the surfaces are in contact, and can be much larger than the elastic restoring force. The elastic restoring force is generated by the deflection of the SiC cantilever. If the EDF loading is assumed to be only applied near the tip area of the cantilever (which is typically valid with the local drain contact), the effective spring constant of the cantilever can be approximated as $k_{eff} = \frac{E_Y w t^3}{4L^3}$, where E_Y is the Young's modulus. Then the elastic force can be given by $F_{elastic} = k_{eff}(g_0 - g)$, assuming a uniform distance between surfaces, where g_0 is the initial gap between the drain and the beam before deflection. For a SiC cantilever beam with above-mentioned dimensions, when its tip gets displaced by 200 nm (in contact with drain), it experiences an equivalent elastic restoring force of 979 nN (Figure 5). This force changes very little when the gap between surfaces is within a few nanometers, because the total deflection is already around 200 nm. In comparison, the EDF increases dramatically when the distance between surfaces decreases to less than 2 nm. In a SiC NEMS switch, stiction is a complex phenomenon, the modeling of which requires detailed knowledge of the surface geometry of the devices involved. Here we employ a simplified model, where the EDF between the surfaces is dominated by contributions within the contact area between the interfaces, and in the contact area, the surfaces are at atomic distance to each other. As shown in Figure 5, the EDF increases extremely quickly at short distances, so the assumption of dominance of the contact region in EDF is reasonable. Assuming the distance between two contacting surfaces cannot be smaller than the lattice constant of SiC which is 4.36 Å, then when the two surfaces are in contact, the largest EDF per unit area is 8.3×10^7 Pa, which leads to an EDF of 2.1×10^{-5} N, assuming a contact area of 0.25 μm². This EDF is more than 20 times of the elastic restoring force, leading to permanent stiction. A second assumption is to extrapolate Lifshitz formula results to atomically close contact surfaces.

Strictly speaking, at such distances a fully quantum mechanical many-body model is needed to calculate the force between the surface areas. Nonetheless, Lifshitz model is often used as a good starting point to estimate the EDF between contact surfaces, and it is known to be consistent with the microscale Lennard-Jones potential used to model the interaction between atoms.

To cause stiction in a SiC NEMS switch discussed in the previous paragraph, it only needs enough contact area A_C so that the force due to this electrodynamic pressure is larger than the elastic restoring force. The resulting contact area between atomically smooth surfaces is the shockingly small $A_C \approx 0.012$ μm². For a typical NEMS switch with contact area of $A_C = 0.25$ μm², this represents only around 5% of the nominal contact area. Even when surface roughness reduces the actual contact that can be treated as atomically close, this represents an extremely low threshold for stiction due to EDF. Other short-range forces can also contribute to the stiction, together with EDF. Moisture condensation force can be mitigated by optimizing the measurement environment, and electrostatic force can be minimized by reducing the bias voltage between the cantilever and the local drain contact, but EDF is always present and is fundamental, independent of the device operating or packaging environment. In essence, intermolecular forces and Casimir/EDF forces are the two special cases or extremes of the same, single force, one at the individual molecule level (intermolecular forces), and the other at the level where we can approximate each of the interacting objects as a continuum rather than consisting of individual molecules (EDF). Mesoscopic devices such as our SiC NEMS switches can be treated using the latter approximation. With EDF alone, the threshold for stiction between two surfaces in NEMS switches is already well above 1 nm, where the other forces are less important; and because EDF is long range, it will be the dominant force. Even if we take other forces into consideration, the threshold value of gap for stiction will only be larger.

To mitigate the stiction problem caused by EDF between smooth, closely spaced surfaces, we propose to create artificial grooves to engineer more roughness in the surface, and systematically reduce the contact area. A schematic of the 1D sinusoidal grooves that can be patterned onto one of the two contacting surfaces is illustrated in **Figure 6**a. When the grooved surface is in contact with a flat surface (Figure 6b), the gap d becomes the atomic distance between the contact surfaces (assumed to be the lattice constant), a is the magnitude or depth of the surface modulation, and λ is the spatial period of the grooves. The EDF between a grooved surface and a flat surface can be treated using the so-called Derjaguin approximation, if the radius of curvature of the surface near contact is much larger than the smallest gap distance d.[48–50] This is satisfied when $d \ll \frac{\lambda^2}{4\pi^2 a}$ or $\frac{\lambda^2}{4\pi^2 ad} \gg 1$, and to satisfy this condition, we take $\lambda^2/(4\pi^2 ad) = 10 \gg 1$. As we will show in Equation (6) below, the reduction of the EDF from grooves does not depend on λ, so this condition can be satisfied independent of the need of reducing stiction, by using a relatively large λ. In this approximation, the electrodynamic energy is computed by summing up piece-wise electrodynamic energy between the facing surface segments. Because EDF rapidly
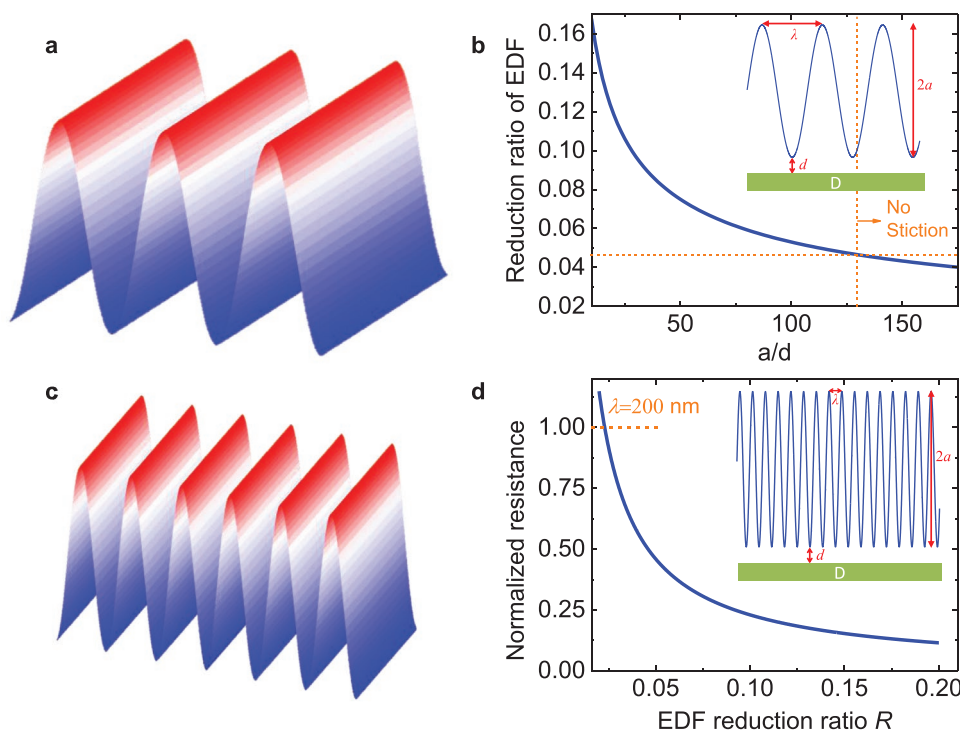
Figure 6. Proposed grooved surface to reduce stiction. a) A 3D schematic of the proposed sinusoidal groove surface. b) Calculated reduction ratio of EDF using the proposed sinusoidal grooves on one of the contacting surfaces at different groove geometries, to the EDF between two parallel plates without grooves at a distance d. Inset: the geometric parameters. d is fixed at the interatomic distance ($d = 0.436$nm), a/λ^2 is kept constant while a is swept (i.e., λ is varied accordingly), which ensures $\lambda^2/(4\pi^2 ad) = 10$. c) A 3D schematic of the proposed sinusoidal groove surface with smaller groove period and thus smaller contact resistance. d) Calculated contact resistance normalized to the case when period $\lambda = 200$ nm, to satisfy $\lambda^2/(4\pi^2 ad) \gg 1$. Inset: illustration of grooves with smaller λ, and geometric parameters when in contact with a flat plate.

declines with longer distance, the dominant contribution of the force comes from the regime where the EDF takes the form of $F = Hg^{-3}$, and the pairwise energy is therefore Hg^{-2}.

Under the Derjaguin approximation, the interaction energy between the grooved and smooth surface over half of a period is:[43–45]

$$E = H \int_0^{\frac{\lambda}{2}} \frac{dx}{\left(d + a + a\cos\frac{2\pi x}{\lambda}\right)^2} = \frac{A\lambda}{2} \frac{a+d}{\left[(a+d)^2 - a^2\right]^{3/2}} \quad (4)$$

The force between the plates can then be easily computed by taking the derivative against distance d:

$$F_{\text{groove}} = \frac{\partial E}{\partial d} = -\frac{H\lambda}{2} \frac{2(a+d)^2 + a^2}{\left[(a+d)^2 - a^2\right]^{5/2}} \approx \frac{3H\lambda}{8\sqrt{2}} a^{-1/2} d^{-5/2} \quad (5)$$

In the last step we made an approximation assuming $d \ll a$, which is typically true because the lattice constant is much smaller than the patterned features. Comparing EDF from a grooved surface with that of a smooth surface, both at distance d away from a contacting smooth and flat surface, the EDF is reduced by ratio R:

$$R = \frac{F_{\text{groove}}}{F_{\text{smooth}}} = \frac{3}{4\sqrt{2}} \sqrt{\frac{d}{a}} \quad (6)$$

The range of this force reduction using a grooved surface for different a/d ratio is shown in Figure 6b. When $d = 4.36$ Å, a groove that is $2a = 26$ nm deep can already result in a reduction of EDF by an order of magnitude, which means that if the initial smooth surface is 0.12 μm² (500 nm × 240 nm), then after using a grooved surface, the elastic restoring force can already balance the EDF and avoid stiction. If the initial smooth surface is still 0.25 μm², then a groove depth of $2a = 113$ nm can ensure the balance between the elastic force and EDF. With an even larger groove depth a, the EDF can be further reduced to 4% or even lower, compared with that between two smooth surfaces. This calculation demonstrates that deliberately engineered surface roughness can greatly reduce the chance of stiction. The dependence of $\sqrt{\frac{d}{a}}$ ensures that even if a changes a little due to some wearing out from mechanical switching, the EDF reduction ratio does not change dramatically and can still result in a much reduced EDF. The multiple contact lines also ensure enough current carrying capability. Of course, real device surfaces are not atomically smooth as assumed in our calculation of F_{smooth}, so the actual force reduction is not so dramatic. In fact, when surface roughness is considered, the EDF will be further reduced on top of the reduction with the grooves, which further avoids stiction and device failure. Rectangular ridges between metallic surfaces have been experimentally demonstrated to reduce the EDF, and discrepancy of more than a factor of two is found when comparing the experimental result with the

ADVANCED
SCIENCE NEWS
www.advancedsciencenews.com

NANO · MICRO
small
www.small-journal.com

calculation of the EDF for patterned surfaces.[51] The measured force is smaller than the calculation result, suggesting a larger EDF reduction than the calculation. In our SiC NEMS switches, we expect some similar effect and we are likely underestimating the reduction of Casimir force due to the engineered grooves.

Besides the EDF reduction, the contact resistance is also very important for NEMS switches. When the grooved surface is used, the contact area will inevitably be smaller compared with that of smooth surfaces, leading to a larger contact resistance. Therefore, there is a tradeoff between EDF reduction and contact resistance compromise. Because $\lambda^2/(4\pi^2 ad) \gg 1$ is required for the Derjaguin approximation to be used for grooved surfaces,[43–45] here we let $\lambda^2/(4\pi^2 ad) = 10 \gg 1$, so $\lambda = \frac{3\sqrt{5}\pi d}{2R}$, where R is the EDF reduction ratio. When the surfaces are in contact, d is the interatomic distance $d = 4.36$ Å. To reduce the contact resistance, λ should be as small as possible so that within certain contact area, there are more contact lines/regions for boosting current flow and conduction (Figure 6c); but this will also mean less EDF reduction (Figure 6d). This tradeoff provides important guidelines for designing M/NEMS switches that can not only use surface engineering to reduce the risk of stiction, but also pursue smaller contact resistance. Although the reduction of contact area may induce larger contact resistance, the stiction is a more severe problem in NEMS switches because it can lead to device failure after only a few cycles. The contact resistance can be improved by doping the SiC more heavily or by depositing a thin layer of metal (not between the contact surfaces). Even with a relatively large contact resistance, the NEMS switches can still be useful for a number of applications, such as power gating and management, high-temperature logic and power electronics, or in ultralow-power applications where switching events are infrequent and high speed may not be necessary.

In the previous calculation for two smooth and flat surfaces, we assume that the contact area is the same as the overlapping area between the cantilever and the local drain. This is true for two parallel plates, but may not be necessarily true for the cantilever because when the cantilever deflects, it may not be parallel with the local drain. To obtain the details of the cantilever beam deflection profile, we perform FEM simulation. As shown in **Figure 7**a,b, for a cantilever with $L = 8$ μm, $w = 200$ nm, $t = 500$ nm, $L_C = 500$ nm, gate-to-beam distance $g_{GS} = 300$ nm, and drain-to-beam distance $g = 200$ nm, the cantilever shows different deflection profiles at different V_G. At larger gate voltages, the beam is almost flat at the contact region, leading to a large contact area, because the large electrostatic force pulls the beam down to make strong contact with the local drain. In real devices, the mechanical pull-in effect will further enhance this contact area because when the beam suddenly contacts the drain, the beam will keep deflecting due to the momentum, and will likely form full contact with the local drain, which can be confirmed by the SEM image in Figure 1e. This can even lead to the beam contacting the gate if the g_{GS} is equal to g, further increasing the chance of stiction (red line in Figure 7b). To avoid the beam contacting the gate, we design g_{GS} to be slightly larger than g. In this case, the beam will not contact the gate, but the contact area with the drain can still be very large. Therefore, the assumption that the contact area being the same as the overlapping area between the cantilever and the local drain is reasonable in many cases during NEMS switch operation, thus our proposed EDF reduction technique using surface grooves is necessary for avoiding stiction and extending the lifetime of NEMS switches.

To examine and verify the EDF reduction using grooved surfaces in realistic devices, we also perform FEM simulation on a SiC NEMS switch with experimentally relevant geometry and a grooved surface. We use a sinusoidal groove depth of $2a = 100$ nm and a spatial period $\lambda = 110$ nm on the beam (Figure 7c). As a comparison, we also simulate a cantilever with a flat surface (Figure 7d). When the grooved cantilever deflects toward the drain contact and the distance is very close, the EDF is dominated by $F = Hg^{-3}$ in the area that is closer to the drain. Due to the beam deflection profile with a small slope, the EDF per unit area not only periodically changes according to the sinusoidal grooves, but also decreases as the location on the cantilever is further away from the tip (Figure 7e). By comparing the EDF between two flat surfaces and the EDF between a grooved and a flat surface, we find that although the maximum values of EDF per unit area are very similar, the majority portion of the grooved surface has minimal EDF per unit area, thus leading to a greatly reduced EDF. From this approximate but realistic simulation, we clearly observe the advantage of using the grooved surfaces for reducing the chance of stiction. Because the SiC NEMS switch is fabricated using top-down lithography techniques followed by dry etching, and the grooves are on the sidewall of the SiC cantilever, these surface grooves could be potentially fabricated with high-fidelity patterning and etching. While we use sinusoidal grooves as a demonstration, other patterns with potentially better EDF reduction, such as trapezoidal grooves, can be explored by the same top-down nanofabrication techniques.

When surface roughness is considered, the EDF can be further reduced. The polycrystalline SiC has surface roughness $R_a \approx 8$ nm, and this applies to both flat surfaces and surfaces with artificially engineered grooves.[7] As a first-order approximation, the surface roughness can be implemented as very shallow sinusoidal variations or perturbations superposed on top of the designed grooves. According to our analysis, for a typical SiC NEMS switch with overlapping contact region of 0.25 μm^2 and without considering the surface roughness, we will need a sinusoidal groove with the depth of $2a = 113$ nm to avoid stiction. This is much larger than the natural roughness of the surface, so the surface roughness alone is not enough to avoid stiction in many cases. But when surface roughness is added to the engineered sinusoidal grooves (Figure 7f), the EDF can be further reduced, which is beneficial for avoiding stiction (Figure 7g). Since the surface grooves are usually deeper compared with surface roughness, these deeper grooves help reduce the EDF efficiently, while the contact resistance will not change very much because it is more determined by the asperities and the regions in actual contact, which are smaller than the characteristic dimensions of the grooves.

3. Conclusion

In summary, we report theory-grounded estimations of the EDF for both gold and SiC parallel plates by employing the full
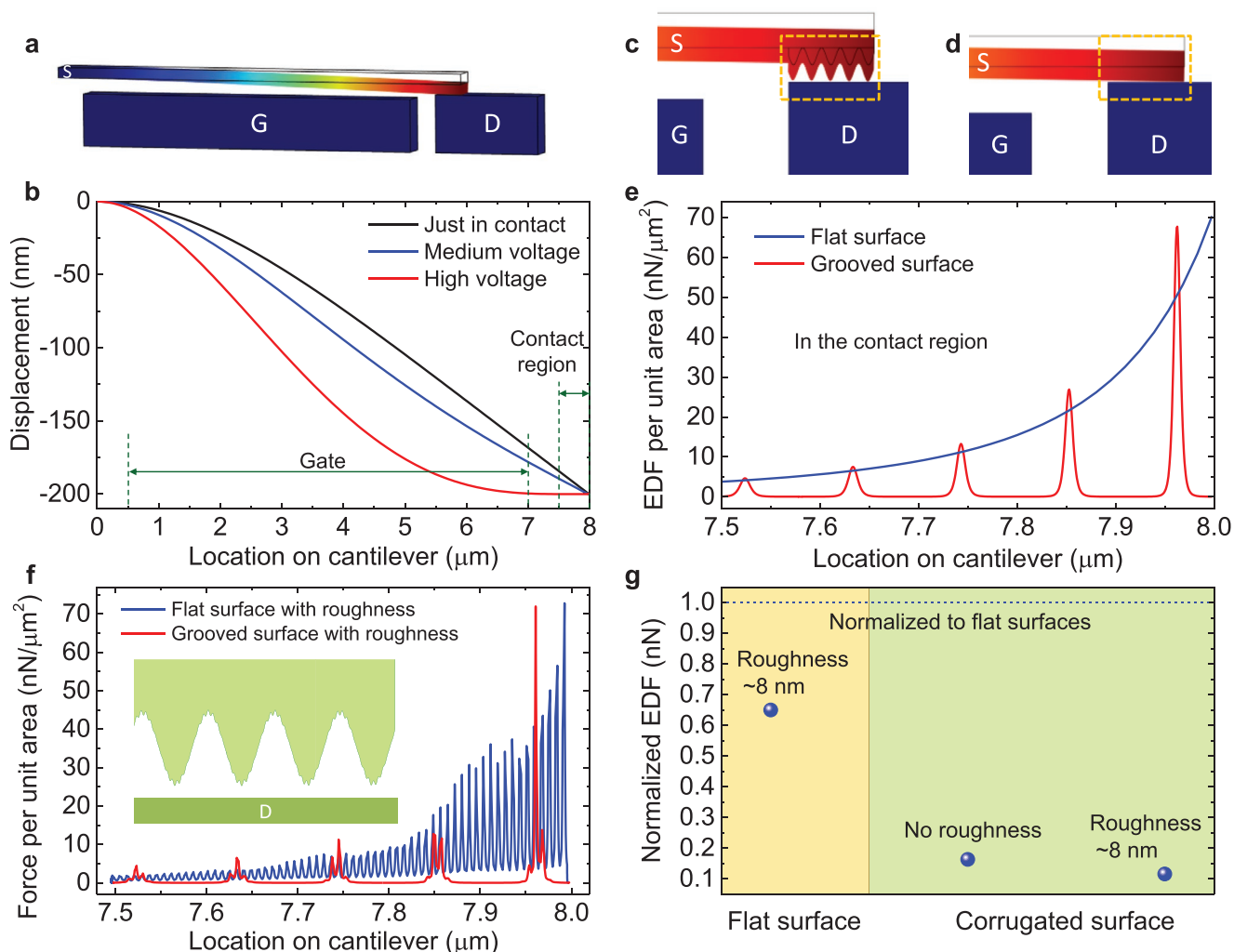
ADVANCED
SCIENCE NEWS
www.advancedsciencenews.com

NANO · MICRO
small
www.small-journal.com

Figure 7. FEM simulation of the deflection profile and the EDF reduction from the grooved surface, for SiC cantilever NEMS switches with $L = 8$ µm, $w =$ 200 nm, $t = 500$ nm, $L_C = 500$ nm, and $g_{GS} = 300$ nm. a) Simulated 3D deflection in color scale showing the contact between the cantilever beam and the drain. b) Simulated beam deflection profile for a switch with $g = 200$ nm at different V_G during NEMS switching, showing the contact area that generates EDF. c,d) Simulated deflection profiles of the SiC NEMS switches with initial $g = 100$ nm without considering the surface roughness, for cantilevers with c) grooved surface, and d) flat surface, right before the beam makes contact with the drain (the closest distance is around 5 nm). e) Comparison of simulated EDF per unit area for grooved surface and flat surface along the cantilever, in the contact region shown by the dashed boxes in (c) and (d). f) Comparison of the simulated EDF per unit area when surface roughness of $R_a \approx 8$ nm is considered, for both grooved surface and flat surface along the cantilever sidewall. Inset: Illustration of a surface with sinusoidal grooves and superposed surface roughness (much smaller sinusoidal perturbations with smaller periods). g) Comparison of simulated EDF between a smooth surface and a flat surface with roughness of $R_a \approx 8$ nm (orange background), and corrugated surfaces (green background) without considering roughness and with roughness of $R_a \approx 8$ nm, with these forces normalized to EDF for flat, ideally smooth surface.

Lifshitz formula and propose grooved surfaces for reducing the EDF. With experimental observation of SiC NEMS switch stiction problem, we estimate the EDF and the restoring force using realistic device parameters, and prove that EDF-induced stiction is difficult to avoid in NEMS switches assuming atomically smooth contact surfaces. To reduce the EDF and save the NEMS switches from stiction, we propose a surface engineering technique using sinusoidal grooves on one surface. Our estimations show that the EDF can be reduced by up to 25 times compared with smooth surfaces, and the reduction may be even larger in real devices. The EDF reduction effect is also verified with FEM simulations using experimentally relevant parameters

and geometry, and considering the effects of surface roughness. This study provides a promising engineering technique to decrease the chance of stiction in NEMS switches and extend their lifetime, toward high-temperature and low-power logic applications.

4. Experimental Section

SiC NEMS Switch Fabrication Process: Following the polycrystalline SiC film growth on oxidized silicon wafer as detailed in refs. [9,42], a very thin gold layer (10–15 nm thick) was thermally evaporated on the whole wafer, which functioned as the charge dissipation layer during the

**ADVANCED
SCIENCE NEWS**

www.advancedsciencenews.com

**NANO · MICRO
small**

www.small-journal.com

following EBL processes. Then 170 nm thick polymethyl methacrylate (PMMA) was spin coated as the EBL resist. EBL was then performed to define the NEMS switch geometry, and after developing the resist, a 40 nm thick nickel film was evaporated as a hard etching mask for SiC. SiC was then etched with inductively coupled plasma (ICP) etching using SF_6 and Ar gas, followed by nickel removal in the nickel etchant. Finally, the cantilever beams were suspended by vapor HF etching of the SiO_2 sacrificial layer. Such top-down fabrication process was suitable for extending to the fabrication of the proposed grooved structures, with potential optimization of the lithography and etching processes.

SiC NEMS Switch Measurement: The electrical characterization of the SiC NEMS switch was performed at room temperature in ambient air, using Keithley 4200SCS semiconductor parameter analyzer connected to a probe station. The gate voltage and drain voltage were applied using source measurement units (SMUs), with the source electrode (cantilever beam) grounded. The gate voltage first swept up, and then swept back, with a constant voltage bias at the drain, and the gate and drain currents were monitored throughout the process to show the hysteresis during switching or stiction events.

FEM Simulation of the NEMS Switches: FEM simulation was performed using COMSOL multiphysics software, with the electromechanics module. The SiC Young's modulus was assumed to be $E_Y = 401$ GPa, the Poisson's ratio was $\nu = 0.168$, the mass density was $\rho = 3216$ kg/m^3, and the relative permittivity was $\varepsilon_r = 9.7$. A medium of air or vacuum surrounded the whole NEMS switch structure. The gate, drain, and one end of the cantilever beam were fixed, while the cantilever could move due to the electrostatic force. The contact pair was defined between the cantilever and the local drain electrode surfaces.

Precise EDF Calculation: The electrodynamic interaction energy per unit area for two semi-infinite plates was calculated using Equation (1), and then the EDF was calculated via Equation (2) by taking the derivative. To evaluate the EDF, the dielectric function at imaginary frequencies, which was calculated from the Kramers–Kronig relationship using Equation (3), by using the imaginary part of the dielectric response function $\varepsilon_2(\omega_R)$ at real frequencies ω_R as the input. The $\varepsilon_2(\omega_R)$ data were obtained from experiments for gold and ab initio calculations for SiC, as shown in Figure 3. Then the EDF per unit area and total EDF for gold and SiC were calculated, for two atomically smooth flat surfaces in parallel with each other. To calculate the EDF between one surface with engineered sinusoidal grooves and one flat surface, Derjaguin approximation was used,[43–45] assuming the radius of curvature of the surface near contact was much larger than the smallest gap distance d, which was typically true because d was usually assumed to be the lattice constant. The interaction energy between the grooved and smooth surface over half of a period was calculated with Equation (4), and then the EDF could be calculated by taking the derivative using Equation (5). Assuming that the groove depth is much larger than d, the reduction ratio by etching the sinusoidal grooves compared with two atomically smooth surfaces was calculated using Equation (6).

Acknowledgements

Conflict of Interest

The authors declare no conflict of interest.

[1] M. L. Roukes, in *Proc. IEEE Int. Electron Devices Meeting (IEDM 04)*, San Francisco, CA **2004**, p. 539.

[2] V. Pott, H. Kam, R. Nathanael, J. Jeon, E. Alon, T.-J. King Liu, *Proc. IEEE* **2010**, *98*, 2076.

[3] Y. Lin, W. Li, Z. Ren, C. T.-C. Nguyen, in *Proc. IEEE Int. Freq. Contr. Symp. (IFCS 08)*, Honolulu, HI **2008**, p. 640.

[4] Y. Hayamizu, T. Yamada, K. Mizuno, R. C. Davis, D. N. Futaba, M. Yumura, K. Hata, *Nat. Nanotechnol.* **2008**, *3*, 289.

[5] S. Chong, B. Lee, S. Mitra, R. T. Howe, H.-S. P. Wong, *IEEE Trans. Elect. Dev.* **2012**, *59*, 255.

[6] P. X.-L. Feng, in *Proc. IEEE Int. Conf. on IC Design & Tech. (ICICDT)*, Leuven, Belgium **2015**, p. 1. https://doi.org/10.1109/ICICDT.2015.7165878

[7] T.-H. Lee, S. Bhunia, M. Mehregany, *Science* **2010**, *329*, 1316.

[8] X.-L. Feng, M. H. Matheny, C. A. Zorman, M. Mehregany, M. L. Roukes, *Nano Lett.* **2010**, *10*, 2891.

[9] T. He, V. Ranganathan, R. Yang, S. Rajgopal, S. Bhunia, M. Mehregany, P. X.-L. Feng, in *Proc. 17th Int. Conf. on Solid-State Sensors, Actuators and Microsystems (Transducers 13)*, Barcelona, Spain **2013**, p. 669.

[10] J. Yaung, L. Hutin, J. Jeon, T.-J. K. Liu, *J. Microelectromech. Syst.* **2014**, *23*, 198.

[11] R. Yang, T. He, M. A. Tupta, C. Marcoux, P. Andreucci, L. Duraffourg, P. X.-L. Feng, *J. Micromech. Microeng.* **2015**, *25*, 095014.

[12] J. N. Israelachvili, *Intermolecular and Surface Forces*, 3rd ed., Elsevier, Amsterdam **2011**.

[13] A. W. Rodriguez, F. Capasso, S. G. Johnson, *Nat. Photonics* **2011**, *5*, 211.

[14] L. M. Woods, D. A. R. Dalvit, A. Tkatchenko, P. Rodriguez-Lopez, A. W. Rodriguez, R. Podgornik, *Rev. Mod. Phys.* **2016**, *88*, 045003.

[15] K. Y. Fong, H.-K. Li, R. Zhao, S. Yang, Y. Wang, X. Zhang, *Nature* **2019**, *576*, 243.

[16] S. Paladugu, A. Callegari, Y. Tuna, L. Barth, S. Dietrich, A. Gambassi, G. Volpe, *Nat. Commun.* **2016**, *7*, 11403.

[17] F. Capasso, J. N. Munday, D. Iannuzzi, H. B. Chan, *IEEE J. Sel. Top. Quant.* **2007**, *13*, 400.

[18] S. K. Lamoreaux, *Rep. Prog. Phys.* **2005**, *68*, 201.

[19] M. Bordag, U. Mohideen, V. M. Mostepanenko, *Phys. Rep.* **2001**, *353*, 1.

[20] N. G. V. Kampen, B. R. A. Nijboer, K. Schram, *Phys. Lett. A* **1968**, *26*, 307.

[21] B. W. Ninham, V. A. Parsegian, G. H. Wiess, *J. Stat. Phys.* **1970**, *2*, 323.

[22] T. Emig, R. L. Jaffe, M. Kardar, A. Scardicchio, *Phys. Rev. Lett.* **2006**, *96*, 080403.

[23] M. T. H. Reid, A. W. Rodriguez, J. White, S. G. Johnson, *Phys. Rev. Lett.* **2009**, *103*, 040401.

[24] S. J. Rahi, T. Emig, N. Graham, R. L. Jaffe, M. Kardar, *Phys. Rev. D* **2009**, *80*, 085021.

[25] A. P. McCauley, A. W. Rodriguez, J. D. Joannopoulos, S. G. Johnson, *Phys. Rev. A* **2010**, *81*, 012119.

[26] J. R. Rodrigues, A. Gusso, F. S. S. Rosa, V. R. Almeida, *Nanoscale* **2018**, *10*, 3945.

[27] K. F. Wang, B. L. Wang, *Nanotechnology* **2019**, *30*, 085502.

[28] S. de Man, K. Heeck, R. J. Wijngaarden, D. Iannuzzi, *Phys. Rev. Lett.* **2009**, *103*, 040402.

[29] W. J. Kim, A. O. Sushkov, D. A. R. Dalvit, S. K. Lamoreaux, *Phys. Rev. A* **2010**, *81*, 022505.

[30] H. B. Chan, V. A. Aksyuk, R. N. Kleinman, D. J. Bishop, F. Capasso, *Science* **2001**, *291*, 1941.

[31] F. Intravaia, S. Koev, I. W. Jung, A. A. Talin, P. S. Davids, R. S. Decca, V. A. Aksyuk, D. A. R. Dalvit, D. López, *Nat. Commun.* **2013**, *4*, 2515.

[32] C. Wagner, N. Fournier, V. G. Ruiz, C. Li, K. Mullen, M. Rohlfing, A. Tkatchenko, R. Temirov, F. S. Tautz, *Nat. Commun.* **2014**, *5*, 5568.

[33] J. Munday, F. Capasso, V. A. Parsegian, *Nature* **2009**, *457*, 170.

[34] A. W. Rodriguez, A. P. McCauley, D. Woolf, F. Capasso, J. D. Joannopoulos, S. G. Johnson, *Phys. Rev. Lett.* **2010**, *104*, 160402.

[35] J. Zou, Z. Marcet, A. W. Rodriguez, M. T. H. Reid, A. P. McCauley, I. I. Kravchenko, T. Lu, Y. Bao, S. G. Johnson, H. B. Chan, *Nat. Commun.* **2013**, *4*, 1845.

[36] L. Tang, M. Wang, C. Y. Ng, M. Nikolic, C. T. Chan, A. W. Rodriguez, H. B. Chan, *Nat. Photon.* **2017**, *11*, 97.

[37] E. D. Palik, *Handbook of Optical Constants of Solids*, Elsevier Inc., Amsterdam **1997**.

[38] G. L. Harris, *Properties of Silicon Carbide*, INSPEC, The Institution of Electrical Engineers, London **1995**.

[39] W. R. L. Lambrecht, B. Segall, *Phys. Rev. B* **1994**, *50*, 10722.

[40] S. Logothetidis, J. Petalas, *J. Appl. Phys.* **1996**, *80*, 1768.

[41] P. T. B. Shaffer, *Appl. Opt.* **1971**, *10*, 1034.

[42] T. He, R. Yang, V. Ranganathan, S. Rajgopal, M. A. Tupta, S. Bhunia, M. Mehregany, P. X.-L. Feng, in *Proc. IEEE Int. Electron Devices Meeting (IEDM 13)*, Washington, DC **2013**, p. 108.

[43] V. B. Svetovoy, *Phys. Rev. B* **2008**, *77*, 035439.

[44] M. Sedighi, V. B. Svetovoy, W. H. Broer, G. Palasantzas, *Phys. Rev. B* **2014**, *89*, 195440.

[45] M. Sedighi, V. B. Svetovoy, G. Palasantzas, *Phys. Rev. B* **2016**, *93*, 085434.

[46] P. Ball, *Nature* **2007**, *447*, 772.

[47] V. B. Svetovoy, A. V. Postnikov, I. V. Uvarov, F. I. Stepanov, G. Palasantzas, *Phys. Rev. Appl.* **2020**, *13*, 064057.

[48] W. Yan, K. Komvopoulos, *J. Appl. Phys.* **1998**, *84*, 3617.

[49] F. W. Delrio, M. P. de Boer, J. A. Knapp, E. D. Reedy Jr., P. J. Clews, M. L. Dunn, *Nat. Mater.* **2005**, *4*, 629.

[50] K. Komvopoulos, *Wear* **1996**, *200*, 305.

[51] F. Intravaia, S. Koev, I. W. Jung, A. A. Talin, P. S. Davids, R. S. Decca, V. A. Aksyuk, D. A. R. Dalvit, D. Lopez, *Nat. Commun.* **2013**, *4*, 2515.